JOURNAL OF MOLECULAR SPECTROSCOPY 99, 263–278 (1983)

Ab Initio Rovibrational Spectrum of LiNC and LiCN

GEERT BROCKS AND JONATHAN TENNYSON[1]

Instituut voor Theoretische Chemie, Katholieke Universiteit, Toernooiveld, 6525 ED Nijmegen, The Netherlands

Rovibrational calculations are performed on an ab initio potential energy surface for lithium cyanide. Vibrational states localized about both the isocyanide structure and the metastable cyanide structure are found. Calculated fundamental frequencies are LiNC 126.6 cm^{-1} (bend) and 754.3 cm^{-1} (stretch); LiCN 165.8 cm^{-1} (bend) and 688.8 cm^{-1} (stretch). Many states are found in the region of the barrier to isomerization, some of which are delocalized (polytopic).

1. INTRODUCTION

The alkali metal cyanides have potential energy surfaces which are insensitive, compared to conventional molecules, to the angle between the metal and the cyanide. This gives rise to several interesting properties. Solid *M*CN (*M* = Li, Na, K, etc.) compounds undergo a phase change between a low temperature ordered phase and a disordered one in which the cyanide ions are randomly oriented throughout the crystal. In the gas phase, these cyanides have a large amplitude bending motion and the equilibrium structure varies according to the size of the metal ion (*1*).

Experimental (*2, 3*) and theoretical (*4–6*) work has shown KCN and NaCN to be triangular with low barriers to internal rotation, especially at the isocyanide structure. Recent rovibrational calculations on KCN (*7–9*) have shown the use of Watson's Hamiltonian for bent molecules (*10*) to be inappropriate because of the lowness of this barrier. These calculations were performed on an ab initio potential energy surface (*4*) and gave fair agreement with the sketchy experimental data available (*9*). In contrast, earlier dynamical calculations on KCN used model potential surfaces which have been found to be in error. Those of Istomin *et al.* (*11*) were based on a linear KNC equilibrium structure. Bunker and Howe (*12*) used a realistic equilibrium structure but obtained a bending fundamental a factor of two too small because the barrier (500 cm^{-1}) was assumed to be equal for KCN at KNC.

Ab initio calculations have predicted that lithium cyanide has a linear isocyanide structure (*1, 13–15*). However, the flatness of the surface led Clementi *et al.* to speculate on the presence of low-lying free rotor states which they called "polytopic" (*14*). So far only dynamical calculations using model potentials have been performed on LiNC (*11, 12*). In particular, unlike the potential of Essers *et al.* (*1*), neither model calculation contained a barrier between LiNC and LiCN, and the bending fundamentals predicted by the appropriate calculations in both cases, (*11*) and (*12*) with

[1] Current address: SERC Laboratory, Daresbury, Warrington WA4 4AD, Cheshire, U.K.

0022-2852/83 $3.00

H = 3000 cm^{-1}, were considerably lower than the experimental matrix isolation values (*16*). We know of no rovibrational data on gaseous lithium cyanide.

The ab initio potential energy surface of Essers *et al.* (*1*) has been fitted in a suitable form for dynamical calculations. This surface, like that used for the dynamical studies on KCN (*4*), is a Legendre expansion of the potential from extended basis set SCF calculations. It predicts that linear LiCN lies 2281 cm^{-1} above the absolute minimum at linear LiNC, but that both structures are local minima separated by a barrier of 3377 cm^{-1} (measured from LiNC). The surface is thus flat in the bending coordinate, which is strongly coupled to the Li–CN separation (see Fig. 1). It is possible that both minima support localized rovibrational states. This is similar to the situation in hydrogen cyanide, where both HCN and HNC have been observed (*17*). Dynamical calculations (*11*) on an ab initio potential (*18*) have shown tunneling between HCN and HNC structures to be significant as much as 2000 cm^{-1} below the barrier to isomerization.

In this paper, we apply a method similar to that of Le Roy and co-workers (*19, 20*) and those successfully applied to KCN (*8, 9*) to lithium cyanide. This approach falls into the class of methods recently christened LC-RAMP, linear combination of radial and angular momentum function products (*21*). Unlike methods based upon an equilibrium structure (*7, 10, 22*), it allows us to perform calculations which treat both LiNC and LiCN structures equally. We treat fully the coupling between Li–CN bending and stretching modes, unlike the previous calculation of LiCN (*11, 12*). We can thus determine whether the surface of Essers *et al.* (*1*) supports any states localized about LiCN and at what point tunneling between the isomers becomes significant.

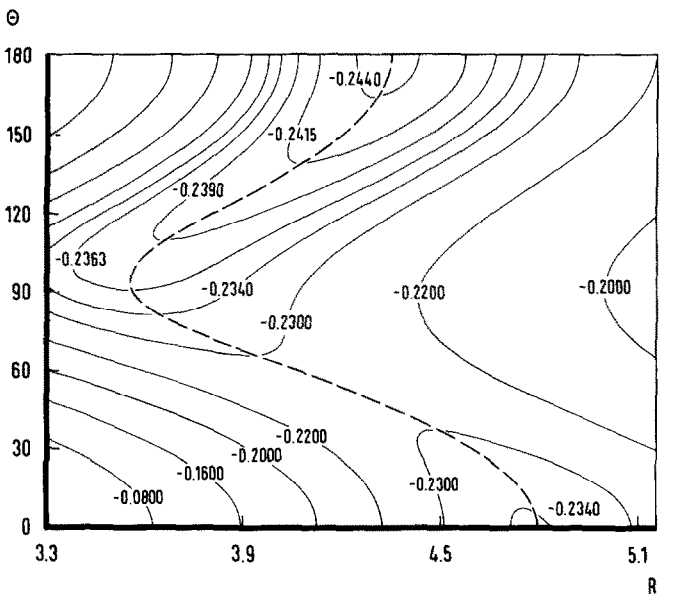

FIG. 1. Potential energy (in a.u.) surface as calculated by Essers *et al.* (*1*). R (in Bohr) is the distance from the CN center of mass to Li, and θ the angle R makes with r(CN). $\theta = 0°$ corresponds to LiCN; $\theta = 180°$ corresponds to LiNC. Dashed line is the path of minimum energy.

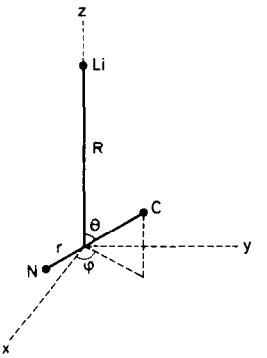

FIG. 2. Body-fixed reference frame.

2. METHOD

Choosing a body-fixed reference frame (see Fig. 2) which has **R**, the vector connecting the CN center of mass with Li, embedded along the z axis and $\mathbf{r} = (r, \theta, \phi)$, the vector from N to C, the Hamiltonian can be written (*20, 23, 24*)

$$\hat{H} = \frac{-\hbar^2}{2\mu_d r}\frac{\partial^2}{\partial r^2} r - \frac{\hbar^2}{2\mu R}\frac{\partial^2}{\partial R^2} R + \frac{\hat{j}^2}{2\mu_d r^2} + \frac{\hat{J}^2 + \hat{j}^2 - 2\hat{\mathbf{j}}\cdot\hat{\mathbf{J}}}{2\mu R^2} + V(r, R, \theta) \tag{1}$$

where $\mu_d^{-1} = m_C^{-1} + m_N^{-1}$ and $\mu^{-1} = m_{Li}^{-1} + (m_N + m_C)^{-1}$. The operator $\hat{\mathbf{j}}$ is the conventional angular momentum operator (*25*) acting on (θ, ϕ). The operator $\hat{\mathbf{J}} = (\hat{J}_x, \hat{J}_y, \hat{J}_z)$ has the form (*11, 24*)

$$\hat{J}_x = \cos\beta \hat{j}_z - \frac{\hbar}{i \sin\beta}\frac{\partial}{\partial\alpha} \tag{2a}$$

$$\hat{J}_y = \frac{\hbar}{i}\frac{\partial}{\partial\beta} \tag{2b}$$

$$\hat{J}_z = \hat{j}_z \tag{2c}$$

$$\hat{J}^2 = \hat{J}_x^2 + \frac{1}{\sin\beta}\hat{J}_y \sin\beta \hat{J}_y + \hat{J}_z^2 \tag{3}$$

where α and β (the polar angles of **R** in a space-fixed system) are the Euler angles defined by the embedding. This Hamiltonian can be transformed into the fully body-fixed form of Tennyson and Sutcliffe (*9*) by performing the final rotation over γ $(=\phi)$ to fix **r** in the x–z plane (*24*).

In this work we make the assumption that the cyanide vibrations are very stiff allowing r to be replaced by r_e, the equilibrium CN bondlength. This approximation is physically reasonable in view of the high frequency of the CN stretching fundamental and has recently been shown to be very good for atom–diatom Van der Waals complexes (*23*). Thus the Hamiltonian of Eq. (1) reduces to

$$\hat{H} = \frac{-\hbar^2}{2\mu R}\frac{\partial^2}{\partial R^2} R + \frac{\hat{j}^2}{2\mu_d r_e^2} + \frac{\hat{J}^2 + \hat{j}^2 - 2\hat{j}_z\hat{J}_z - \hat{j}_+\hat{J}_+ - \hat{j}_-\hat{J}_-}{2\mu R^2} + V(r_e, R, \theta) \tag{4}$$

where

$$\hat{j}_\pm = \hat{j}_x \pm i\hat{j}_y \qquad \hat{J}_\pm = \hat{J}_x \mp i\hat{J}_y. \tag{5}$$

Suitable angular basis functions for this form of the Hamiltonian are (*9*, *20*)

$$Y_{jk}(\theta, \phi)D^J_{Mk}(\alpha, \beta, 0) \tag{6}$$

where D^J_{Mk} is a spherical top eigenfunction and Y_{jk} a spherical harmonic (*25*). The angular matrix elements obtained by $\hat{\mathbf{J}}$ and $\hat{\mathbf{j}}$ acting on these basisfunctions are (*11*, *24*)

$$\hat{J}^2 D^J_{Mk}Y_{jk} = \hbar^2 J(J+1)D^J_{Mk}Y_{jk} \tag{7a}$$

$$\hat{j}_z\hat{J}_z D^J_{Mk}Y_{jk} = \hbar^2 k^2 D^J_{Mk}Y_{jk} \tag{7b}$$

$$\hat{j}_\pm\hat{J}_\pm D^J_{Mk}Y_{jk} = C^+_{jk}C^+_{Jk}D^J_{Mk\pm1}Y_{jk\pm1} \tag{7c}$$

where

$$C^\pm_{lk} = [l(l+1) - k(k\pm1)]^{1/2} \tag{8}$$

Letting $\hat{H}$ act on these basisfunctions, multiplying from the left by $Y^*_{j'k'}D^{J*}_{Mk'}$ and integrating over all the angular coordinates gives the one-dimensional operator

$$\hat{H}^{J,M}_{j'k',jk} = \hbar^2\delta_{k,k'}\delta_{j,j'}\left[\frac{-1}{2\mu R}\frac{\partial^2}{\partial R^2}R + \frac{J(J+1) - 2k^2 + j(j+1)}{2\mu R^2} + \frac{j(j+1)}{2\mu_d r_e^2}\right]$$

$$+ \delta_{k,k'}\langle j'k'|V|jk\rangle_{\theta,\phi} - \frac{\hbar^2}{2\mu R^2}(\delta_{j,j'}\delta_{k',k-1}C^-_{Jk}C^-_{jk} + \delta_{k',k+1}C^+_{Jk}C^+_{jk}) \tag{9}$$

which gives the well-known close-coupled equations (*26*) and for which it is assumed that J and M are good quantum numbers. If the potential is expanded in Legendre polynomials

$$V(R, \theta) = \sum_\lambda V_\lambda(R)P_\lambda(\cos\theta) \tag{10}$$

then the angular integration over the potential can be performed analytically:

$$\langle j'k'|V|jk\rangle_{\theta,\phi,\alpha,\beta} = \sum_\lambda g_\lambda(j', j, k)V_\lambda(R) \tag{11a}$$

$$g_\lambda(j', j, k) = [(2j'+1)(2j+1)]^{1/2}(-1)^k\begin{pmatrix} j' & \lambda & j \\ 0 & 0 & 0\end{pmatrix}\begin{pmatrix} j' & \lambda & j \\ -k & 0 & k\end{pmatrix} \tag{11b}$$

where the $3-j$ symbols in the Gaunt coefficient are standard (*25*).

The angular basis functions of Eq. (6) can be symmetrized according to their behavior under inversion. These symmetrized functions

$$\frac{1}{\sqrt{2}}[D^J_{Mk}Y_{jk} + (-1)^p D^J_{M-k}Y_{j-k}] \qquad p = 0, 1 \qquad k > 0 \tag{12a}$$

$$D^J_{M0}Y_{j0} \qquad p = 0 \qquad k = 0 \tag{12b}$$

have parity $(-1)^{J+p}$ under inversion and allow the problem to be block factorized according to p. In this paper we follow convention (*27*) and label $p = 0$ states e and $p = 1$ states f. This transformation of the basis leaves all the matrix elements of Eq.

(9) unchanged with the exception of a factor of $\sqrt{2}$ outside the final bracket if $k = 0$ or $k' = 0$ (*9*).

Suitable radial functions for $\hat{H}^{JM}_{j'k',jk}$ have the form $R^{-1}\chi_n(R)$ as this removes the R^2 term from the volume element. In this work we follow Le Roy and Van Kranendonk (*19*) and generate our basis functions numerically by solving the pseudodiatomic Schrödinger equation

$$\frac{d^2}{dR^2}\chi_n(R) + \frac{2\mu}{\hbar^2}[E_n - V(R)]\chi_n(R) = 0 \tag{13}$$

which is obtained by setting $j = J = 0$ in the operator of Eq. (8) and letting it act on $R^{-1}\chi_n(R)$. $V(R)$ is a suitable radial potential function; previously V_0, the isotropic part of Eq. (10) (*19*), and $V(R, \theta_e)$ where θ_e is the angle of the equilibrium geometry (*8*), have been used successfully. We return to this in the next section. As LiCN is strongly bound there are more than sufficient bound vibrational states for a saturated radial basis and the use of continuum functions was not considered.

Having generated radial and angular basis sets, we set up the secular matrix of which a general matrix element can be written $\langle n'|\hat{H}^{JM}_{j'k',jk}|n\rangle$ and diagonalize this matrix to obtain our solutions. The bottleneck of this approach is the size of the secular problem encountered especially for rotationally excited states. One approximation which has widely been found useful (*9, 21*) is the neglect of the so-called off-diagonal Coriolis terms. These are the final terms in Eq. (9). Without them, k, the projection of the total angular momentum J on the body-fixed z axis, is a good quantum number and states which differ only by their parity (e or f) become degenerate. Within this approximation it is never necessary to diagonalize secular matrices larger than those required for the rotational ground state. This possibility is a major advantage of the body fixing of the coordinates.

3. ROVIBRATIONAL CALCULATIONS

The LiCN surface of Essers *et al.* (*1*) shows strong coupling between R and θ, and two minima. These properties make rovibrational calculations expensive as large basis sets are required to obtain satisfactory convergence for the energy levels of even the low-lying states. Furthermore, as the two minima are both linear, to obtain even the fundamental vibrational splittings it is necessary to perform both $J = 0$ and $J = 1$ calculations.

To keep the secular problem tractable, it was necessary to employ slightly different basis sets for LiNC, LiCN, and free rotor calculations and we thus discuss each of these separately. We note, however, that these basis sets are not expanded around a particular structure, and thus, for example, the majority of states in the LiCN calculation are in fact localized around LiNC but these LiNC states are not necessarily converged with this basis.

All the calculations presented are for $^7Li^{12}C^{14}N$ with the CN distance fixed at the experimental value of 1.171 Å (2). The numerical solution of Eq. (13) was performed for 1200 steps of 0.00185 Å ($=10^{-3} \times R_e$) from 0.926 Å ($1/2R_e$) outwards. A low value of the convergence criterion (10^{-7} cm^{-1}) was used as larger values were found to cause slight inaccuracies due to nonorthogonality of the radial basis functions.

3.1. LiNC Calculations

Previous calculations on KCN (*8, 9*) required many angular functions to obtain a good representation of several localized states. We followed the usual practice (*8, 9, 20–22*) and included in our basis all possible angular functions with $j \leqq j_{max}$ ($j_{max} + 1$ functions when $J = 0$) and radial functions with $n \leqq n_{max}$ ($n_{max} + 1$ functions).

The 10 lowest $J = 0$ levels are converged to within 0.05 cm^{-1} by an angular basis with $j_{max} = 28$. For higher levels, however, it was necessary to increase j_{max} to 34, at which level we were unable to perform $J = 1$ calculations without neglecting Coriolis interactions.

We had difficulty selecting a suitable potential with which to generate radial basis functions. Use of $V_0(R)$ or $V(R, \theta_f = 180°)$ gave basis sets which were only slowly convergent. This is because in both cases the minimum in the potential is for larger R than encountered in the region $\theta = 70–120°$ where many states have large amplitude. For this reason, the effect of generating the radial basis using cuts through the potential with fixed θ_f at 10° intervals was tested. Figure 3b shows sample results for calculations with $n_{max} = 12$ and $j_{max} = 18$. Radial basis sets generated using

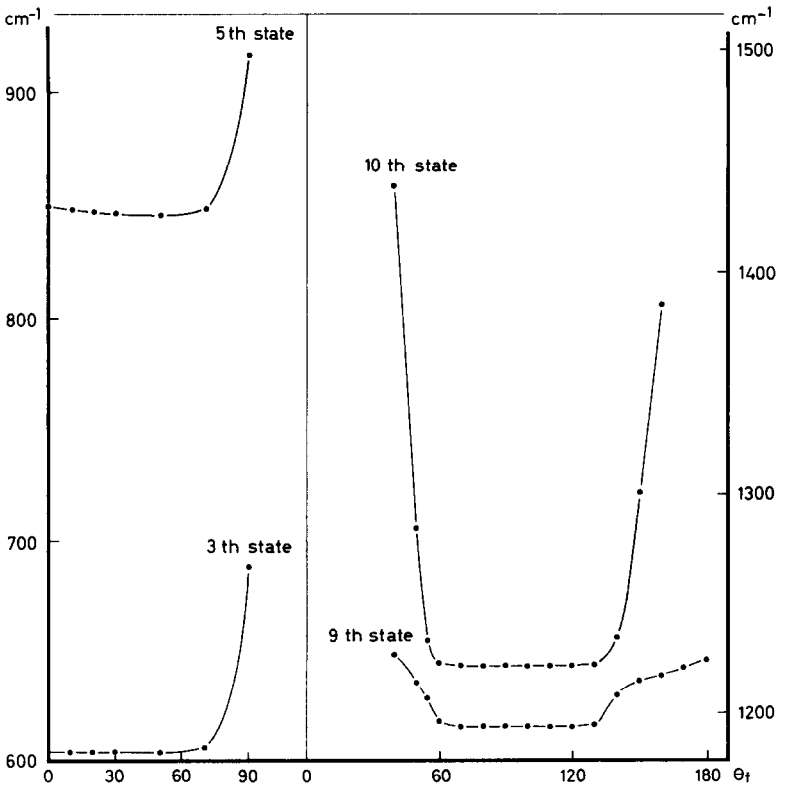

FIG. 3. Variation in energy (in cm^{-1} above ground state) of some localized LiCN(a) and LiNC(b) $J = 0$ states using different radial bases. These bases are generated from different cuts through the potential with fixed θ_f. Results for $n_{max} = 12$ and $j_{max} = 18$.

(9) unchanged with the exception of a factor of $\sqrt{2}$ outside the final bracket if $k = 0$ or $k' = 0$ (*9*).

Suitable radial functions for $\hat{H}^{JM}_{j'k',jk}$ have the form $R^{-1}\chi_n(R)$ as this removes the R^2 term from the volume element. In this work we follow Le Roy and Van Kranendonk (*19*) and generate our basis functions numerically by solving the pseudodiatomic Schrödinger equation

$$\frac{d^2}{dR^2}\chi_n(R) + \frac{2\mu}{\hbar^2}[E_n - V(R)]\chi_n(R) = 0 \tag{13}$$

which is obtained by setting $j = J = 0$ in the operator of Eq. (8) and letting it act on $R^{-1}\chi_n(R)$. $V(R)$ is a suitable radial potential function; previously V_0, the isotropic part of Eq. (10) (*19*), and $V(R, \theta_e)$ where θ_e is the angle of the equilibrium geometry (*8*), have been used successfully. We return to this in the next section. As LiCN is strongly bound there are more than sufficient bound vibrational states for a saturated radial basis and the use of continuum functions was not considered.

Having generated radial and angular basis sets, we set up the secular matrix of which a general matrix element can be written $\langle n'|\hat{H}^{JM}_{j'k',jk}|n\rangle$ and diagonalize this matrix to obtain our solutions. The bottleneck of this approach is the size of the secular problem encountered especially for rotationally excited states. One approximation which has widely been found useful (*9, 21*) is the neglect of the so-called off-diagonal Coriolis terms. These are the final terms in Eq. (9). Without them, k, the projection of the total angular momentum J on the body-fixed z axis, is a good quantum number and states which differ only by their parity (e or f) become degenerate. Within this approximation it is never necessary to diagonalize secular matrices larger than those required for the rotational ground state. This possibility is a major advantage of the body fixing of the coordinates.

3. ROVIBRATIONAL CALCULATIONS

The LiCN surface of Essers *et al.* (*1*) shows strong coupling between R and θ, and two minima. These properties make rovibrational calculations expensive as large basis sets are required to obtain satisfactory convergence for the energy levels of even the low-lying states. Furthermore, as the two minima are both linear, to obtain even the fundamental vibrational splittings it is necessary to perform both $J = 0$ and $J = 1$ calculations.

To keep the secular problem tractable, it was necessary to employ slightly different basis sets for LiNC, LiCN, and free rotor calculations and we thus discuss each of these separately. We note, however, that these basis sets are not expanded around a particular structure, and thus, for example, the majority of states in the LiCN calculation are in fact localized around LiNC but these LiNC states are not necessarily converged with this basis.

All the calculations presented are for $^7Li^{12}C^{14}N$ with the CN distance fixed at the experimental value of 1.171 Å (2). The numerical solution of Eq. (13) was performed for 1200 steps of 0.00185 Å ($=10^{-3} \times R_e$) from 0.926 Å ($1/2R_e$) outwards. A low value of the convergence criterion (10^{-7} cm^{-1}) was used as larger values were found to cause slight inaccuracies due to nonorthogonality of the radial basis functions.

tification is approximate but can easily be made for the low-lying states of Table I by counting the nodes in the wavefunction. Figure 5a illustrates a state for which such an identification is possible.

Plots, like those of Figs. 5–7, show the low-lying LiNC states to be very harmonic in appearance, despite the very large amplitude of the bending mode. This is unlike the situation in KCN where the states rapidly become very anharmonic (*7–9*). The difference is the much larger separation between the bending and stretching fundamentals which results in much purer LiNC states.

Thus, our vibrational fundamentals for LiNC are 126.7 and 754.3 cm^{-1} for v_b and v_s, respectively, and zero point energy 510.8 cm^{-1}.

The only experimental data on lithium cyanide is due to Ismail *et al.* (*16*). They attribute their spectra, taken in rare gas matrices, to LiNC, a conclusion confirmed by a reanalysis of their isotopic substitution data (*30*). Their results for a Ne matrix were $v_b = 119.5$ cm^{-1}, $v_s = 680.5$ cm^{-1} and for an Ar matrix $v_b = 96$ and 134 cm^{-1}, $v_s = 646.6$ cm^{-1}. In view of the large matrix shifts (we note that the Ar matrix splits the degenerate bending mode) the agreement with our levels is better than could be anticipated.

Table I also shows the energies obtained by neglecting the off-diagonal Coriolis interactions. The errors in this approximation are small compared to the vibrational spacing, but nearly four times those for the comparable calculations on KCN (*9*). Calculations which neglect the Coriolis interactions are used for the higher vibrational states.

Table II gives some vibrational averaged geometric data for the $J = 0$ states of Table I. We note steady shift in $\langle\theta\rangle$ with increasing excitation of the bending mode and corresponding decrease in $\langle R\rangle$ (see Fig. 1). The large deviations from the equi-

TABLE II

Calculated $J^p = 0^e \rightarrow 1^e$ Transition Frequencies and Vibrational Averaged Geometric Parameters for the LiNC $J = 0$ Levels of Table I (Equilibrium Values of R and θ are 2.302 Å and 180°)

Level	$J^p = 0^e \rightarrow 1^e/cm^{-1}$		<R>/Å	<θ>[a]
number	Full	No Coriolis		
1	0.8909	1.1605	2.298	168.7°
2	0.9138	1.1873	2.272	159.7°
3	0.9424	1.2204	2.242	152.6°
4	0.9806	1.2623	2.207	145.8°
5	0.8846	1.1496	2.314	168.6°
6	1.0299	1.3163	2.164	138.7°
7	1.0994	1.3840	2.115	131.2°
8	0.9082	1.1766	2.288	159.4°
9	1.1585	1.4368	2.079	125.7°
10	0.9385	1.2116	2.256	151.8°

[a] <θ> = arccos(<cosθ>)

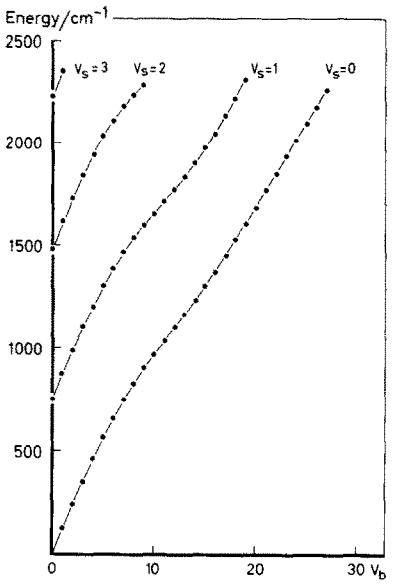

FIG. 4. Energy (in cm^{-1} above ground state) of the lowest vibrational states of LiNC as function of bend (v_b) and stretch (v_s) quantum numbers.

librium at $\theta_e = 180°$ show the bending mode to be very "floppy." Table II also shows the rotational excitation energies calculated including and neglecting the Coriolis interactions. The transition $J^p = 0^e \rightarrow 1^e$ occurs at $2B$. It is also possible to calculate B from the vibrational average $\langle R^{-2} \rangle$ for the corresponding $J = 0$ state. Rotational constants calculated in this fashion are indistinguishable from those calculated neglecting Coriolis interactions. The full calculation, including all Coriolis terms, gives a consistent lowering of the transition energies by about 25% showing that the Coriolis interactions are important in LiNC if accurate rotational transition frequencies are to be calculated.

Next we performed a $J = 0$ calculation using $j_{max} = 34$ and $n_{max} = 13$ ($\theta_f = 110°$). At this level the 30 lowest $J = 0$ states are converged to within 0.1 cm^{-1}, although the 31st shows anomalous behavior. The 30 lowest $J = 0$ states are localized about LiNC and assignments can be made to v_s and v_b. Figure 4 shows their energies plotted according to v_s and v_b.

Above these levels and below the top of the barrier at 3377 cm^{-1} are at least another 38 $J = 0$ states. The majority of these are localized about LiNC having small amplitude on the other side of the barrier. Figure 5 depicts two such states. For some of these states, e.g., Fig. 5a, it is still possible to assign v_s and v_b quantum numbers from the appearance of their nodal structure, but for the majority, e.g., Fig. 5b, this is not possible. Bunker and Howe (*12*) adapted the Yamada–Winnewisser parameter (*31*) to correlate between strongly bent ($\gamma = +1$), strongly linear ($\gamma = -1$), and free internal rotor ($\gamma = -3$) triatomic molecules. They define

$$\gamma_{v_s,v_b} = 1 - 4\left[\frac{E(1, v_s, v_b, 0^e) + E(1, v_s, v_b + 1, 1^e) - 2E(0, v_s, v_b, 0^e)}{E(0, v_s, v_b + 2, 0^e) - E(0, v_s, v_b, 0^e)}\right] \quad (14)$$

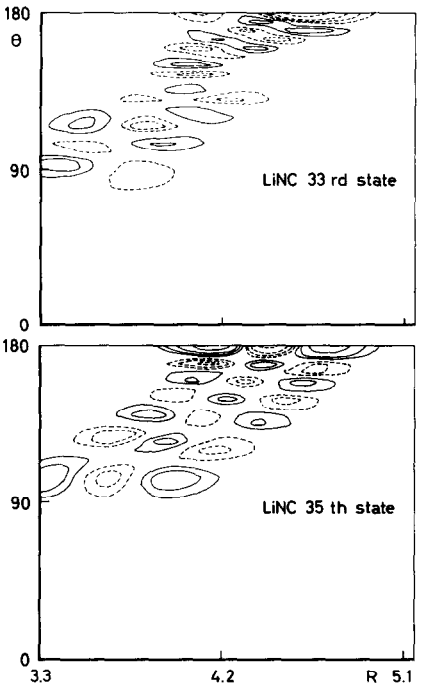

FIG. 5. Two $J = 0$ vibrational wave functions of LiNC (R in Bohr). The contours link points where the wave function has 8, 16, 32, and 64% of its maximum amplitude. Solid curves enclose regions of positive amplitude and dashed curves regions of negative amplitude. (a) The 35th state can be labeled (see text) (J, v_s, v_b, k^p) = (0, 2, 12, 0°). (b) It is impossible to assign bend (v_b) and stretch (v_s) labels for the 33rd state.

using energies labeled by the state labels discussed above. For the 30 lowest LiNC levels, where it is possible to assign v_s and v_b, $\gamma_{v_s v_b}$ remains at about -1.1 showing LiNC to be linear in behavior. For the higher levels, where one might expect a shift towards free rotor states, v_s and v_b cannot, in general, be assigned. This means that in a multidimension (or real world) calculation this parameter is only of limited usefulness.

The 31st $J = 0$ level, which is not well represented by the current basis set, is the first level to show appreciable density at LiCN. Indeed this state is localized in the LiCN region of the surface. Calculations on this and higher LiCN states as well as free rotor states required further adaptations of the basis set and are discussed in the next two subsections.

3.2. *LiCN Calculations*

The minimum in the potential at $\theta = 0°$ lies at larger R than that for $\theta = 180°$. It was necessary to use a different radial basis to converge states localized about $\theta = 0°$. Figure 3 shows the effect of varying θ_f on two LiCN states. Use of a basis set with $\theta_f = 40°$, $j_{max} = 28$ and $n_{max} = 12$ converged the lowest $J = 0$ states with appreciable amplitude at $\theta = 0°$ to within 0.01 cm^{-1}. Table III presents the results of this calculation.

TABLE III

LiCN $J = 0$ and 1 Levels

Level number	Label v_s, v_b, k	J = 0	J = 1		
		e	e	f	No Coriolis
1	0,0,0	0.0	0.76		0.95
	0,1,1		166.55	166.57	166.57
2	0,2,0	319.42	320.20		320.39
	0,3,1		469.05	469.06	469.06
3	0,4,0	603.95	604.75		604.95
	0,5,1		734.15	734.16	734.16
4	1,0,0	688.82	689.58		689.76
	1,1,1		857.67	857.68	857.68
5	0,6,0	846.57	847.22		847.39

Notes: Energies (in cm^{-1}) are relative to the LiCN ground state at $-50\,887.47$ cm^{-1}. See Section 3.1 for an explanation of the labeling.

Our calculations predict LiCN fundamentals of 165.8 cm^{-1} and 688.8 cm^{-1} for the bend and stretch, respectively, and a zero point energy of 516.0 cm^{-1}. Identification of these modes was again made by plotting and assigning nodes; Fig. 6 shows a typical example. Table IV gives rotational transition frequencies and vibrationally averaged geometric parameters for the levels of Table III. The values of $\langle\theta\rangle$ clearly show these states to be localized in the LiCN region.

Again neglecting Coriolis interactions causes an appreciable error in the rotational transition frequencies. However, it is clear that the rotational constants of LiCN are about 20% lower than those of LiNC, a property largely due to the increased separation in the cyanide structure.

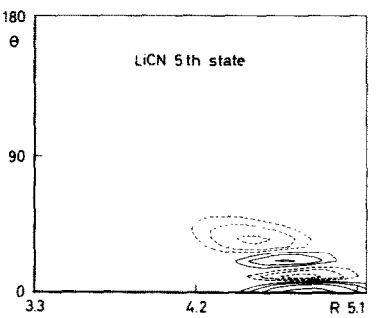

FIG. 6. A $J = 0$ vibrational wave function of LiCN. Contours as in Fig. 5. State labeling: $(J, v_s, v_b, k^p) = (0, 0, 6, 0^e)$.

TABLE IV

Calculated $J^p = 0^e \rightarrow 1^e$ Transition Frequencies and Vibrationally Averaged Geometric Parameters for LiCN $J = 0$ Levels of Table 3 (Equilibrium Values of R and θ are 2.537 Å and 0°)

Level number	$J^p = 0^e \rightarrow 1^e$/cm^{-1}		<R>/Å	<θ>[a]
	Full	No Coriolis		
1	0.7630	0.9462	2.535	9.7
2	0.7791	0.9725	2.510	17.4
3	0.8072	1.0037	2.469	22.4
4	0.7578	0.9449	2.546	10.5
5	0.8353	1.0349	2.436	30.9

[a] <θ> = arccos(<cosθ>)

The fifth $J = 0$ LiCN level still lies 200 cm^{-1} below the barrier to isomerization but already shows appreciable amplitude (5%) on the LiNC side of the barrier. Above this state increasing delocalization makes assignments of any further cyanide states difficult. Indeed, the state which can be identified with the (0, 0, 8, 0^e) LiCN state has a $\langle\theta\rangle$ of 62.8° compared with the barrier at $\theta = 55°$.

Finally, we note that although we have assigned cyanide vibrational states according to the nodal structure of these localized states in the region of the local minimum at $\theta = 0°$, these states must have a complicated nodal structure associated with them in the region $\theta > 55°$. This behavior was clearly demonstrated by Bunker and Howe (*12*) for HNC in one dimension and must also be displayed by our solutions. However, the amplitude of the cyanide given in Table III is typically a factor of 10^4 smaller in the isocyanide region and this behavior is thus hard to detect.

3.3. Free Rotor States

The onset of tunneling is a gradual phenomenon and dependent on near degenjeracies between states localized on opposite sides of the barrier. To investigate the nature of the states in the region of the barrier we performed a brute force calculation with $j_{max} = 44$, $n_{max} = 15$, and $\theta_f = 70°$. This converged the 70 lowest $J = 0$ states to within 2 cm^{-1}. Table V gives the states in the barrier region obtained by this calculation with assignments when possible. As a measure of the degree of tunneling, we give the ratio of the maxima of absolute amplitude on each side of the barrier. Thus for a predominantly isocyanide state, this ratio is $|\psi_{max}(\theta < 55°)/\psi_{max}(\theta > 55°)|$ and for a cyanide state the inverse is given.

What we observe is that while some states below the barrier in energy are significantly delocalized, other higher energy states are still localized. It is thus difficult to predict when free internal rotor or "polytopic" states will occur. Figure 7 shows the amplitude of two typical delocalized states.

It is possible to make assignments, necessarily rather arbitrary, to the eight lowest bending states of LiCN in the $j_{max} = 44$, $n_{max} = 15$ calculation. From these levels

we have calculated $\gamma_{v_s v_b}$. The results are given in Table VI which clearly shows that the highest of these states correlates with a free internal rotor level.

4. CONCLUSIONS

We have obtained the 70 lowest $J = 0$ vibrational states (and corresponding $J = 1$ states) for the ab initio lithium cyanide surface of Essers *et al.* (*1*). The states were found to be generally of three types. The lowest 30 were localized about a linear isocyanide structure and despite the large amplitude bending coordinate were harmonic in appearance. LiNC bending and stretching fundamentals were calculated to lie at 126.6 and 754.3 cm^{-1}, respectively, in agreement with the matrix isolation values (*16*).

The 31st state was found to be localized about the linear cyanide structure. About five $J = 0$ states were found to be localized in this region of the surface. LiCN bending and stretching fundamentals were calculated to lie at 165.8 and 688.8 cm^{-1}, respectively. On this surface LiCN lies 228 cm^{-1} above LiNC (although this difference will be reduced by electron correlation (*15*)) and thus one would expect LiCN to be formed only at high temperature.

TABLE V

$J = 0$ and 1 (No Coriolis) Levels in the Region of the Barrier 3050–3380 cm^{-1}

J = 0					J = 1, k = 1				
Level number	a	Label v_s, v_b	Energy	Relative Amplitude (%)	Level number	a	Label v_s, v_b	Energy	Relative Amplitude (%)
56	NC		3073.2	0.1	53	NC		3086.9	0.3
57	NC	3,12	3101.8	0.5	54	NC		3133.8	4.7
58	CN	0,6	3132.7	4.9	55	CN	1,1	3145.2	0.3
59	NC		3167.2	5.0	56	NC		3160.5	0.7
60	NC	4,2	3185.2	0.2	57	NC		3168.7	0.7
61	NC		3202.2	10.2	58	CN		3231.8	20.8
62	NC		3237.6	4.1	59	NC		3251.2	41.2
63	NC		3245.7	2.1	60	CN	0,7	3272.9	59.4
64	CN	0,8	3297.3	78.5	61	NC		3288.8	0.7
65	CN	1,2	3301.6	17.0	62	CN		3317.6	19.1
66	NC		3333.1	31.5	63	CN		3332.5	23.0
67	CN		3349.0	67.0	64	CN		3368.0	68.6
68	NC	4,4	3376.0	1.0					

Notes: Under heading a, NC/CN denotes that the largest amplitude (and labeling) is around $\theta = 180°/0°$. Energies (in cm^{-1}) are relative to the LiNC ground state at $-53\,173.69$ cm^{-1}. Labels have been assigned when possible. See the text for an explanation of the relative amplitudes.

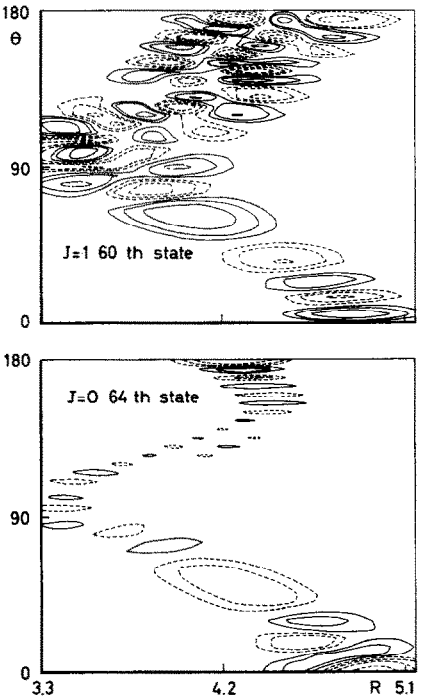

FIG. 7. Two delocalized vibrational states. Contours as in Fig. 5.

Between the 31st state (the LiCN ground state) and the barrier to isomerization at 3377 cm^{-1} we found 37 states. The density of states in this region is high and the natures of individual states vary. Most are predominantly localized about the isocyanide structure, some are localized about cyanide minimum, and several of the higher states are strongly delocalized. These states are the free internal rotor or "polytopic" states discussed by Clementi *et al.* (*14*). However, it is clear that even in the region where completely free internal rotation is energetically possible, many of the states are still localized about one of the two minima.

TABLE VI

Bunker–Howe Correlation Parameter γ (*12*) for the Bending States of LiCN (See Eq. (14). Energies (in cm^{-1}) are Relative to the LiCN Ground State)

v_b	$E(0,0,v_b,0^e)$	$E(1,0,v_b+1,1^e)$	$E(1,0,v_b,0^e)$	γ_{v_b}
0	0.0	166.55	0.76	-1.09
2	319.42	469.05	320.20	-1.12
4	603.95	734.15	604.75	-1.17
6	846.57	986.64	847.22	-2.42
8	1011.07			

All the calculations presented in this work used numerical radial basis sets. Such basis sets have proved excellent for very isotropic problems (*19, 32*), but finding a suitable generating potential gave considerable difficulty in the case of lithium cyanide. Recently an LC-RAMP method has been developed using polynomial rather than numerical basissets (*9*). The parameterization of these basis functions allows them to be optimized by explicit use of the vibrational principle, simplifying the generation of a suitable basis set. This method has been implemented as a fully documented computer program (*33*).

Finally, we note that in the SCF calculations on both LiCN and KCN, the SCF dipole could be well represented by long-range theory (*1, 4*). Work is currently in progress on fitting dipole surfaces for these molecules and using them to calculate vibrationally averaged dipole moments for each state and transition dipoles, giving infrared transition probabilities (*34*).

ACKNOWLEDGMENTS

We thank Professor Ad van der Avoird for his continuous interest in this work, Dr. Brian Sutcliffe for discussions on the Hamiltonian, and Monique Bongers-de Bie for her excellent typing of this manuscript.

Note added in proof. Very recently, lithiumcyanide molecules have, for the first time, been prepared in a molecular beam and their rotational spectrum has been measured (*35*). This spectrum agrees very well with the linear LiNC structure and the $J = 0 \rightarrow 1$ transition frequency predicted by the present calculations.

RECEIVED: November 19, 1982

REFERENCES

1. R. ESSERS, J. TENNYSON, AND P. E. S. WORMER, *Chem. Phys. Lett.* **89,** 223–227 (1982).
2. T. TÖRRING, J. P. BEKOOY, W. L. MEERTS, J. HOEFT, E. TIEMANN, AND A. DYMANUS, *J. Chem. Phys.* **73,** 4875–4882 (1980).
3. J. J. VAN VAALS, W. L. MEERTS, AND A. DYMANUS, *J. Chem. Phys.* **77,** 5245–5246 (1982).
4. P. E. S. WORMER AND J. TENNYSON, *J. Chem. Phys.* **75,** 1245–1252 (1981).
5. M. L. KLEIN, J. P. GODDARD, AND D. G. BOUNDS, *J. Chem. Phys.* **75,** 3909–3915 (1981).
6. C. J. MARSDEN, *J. Chem. Phys.* **76,** 6451–6452 (1982).
7. J. TENNYSON AND B. T. SUTCLIFFE, *Mol. Phys.* **46,** 97–109 (1982).
8. J. TENNYSON AND A. VAN DER AVOIRD, *J. Chem. Phys.* **76,** 5710–5718 (1982).
9. J. TENNYSON AND B. T. SUTCLIFFE, *J. Chem. Phys.* **77,** 4061–4072 (1982).
10. J. K. G. WATSON, *Mol. Phys.* **15,** 479–490 (1968).
11. V. A. ISTOMIN, N. F. STEPANOV, AND B. I. ZHILINSKII, *J. Mol. Spectrosc.* **67,** 265–282 (1977).
12. P. R. BUNKER AND D. J. HOWE, *J. Mol. Spectrosc.* **83,** 288–303 (1980).
13. B. BAK, E. CLEMENTI, AND R. N. KORTZEBOON, *J. Chem. Phys.* **52,** 769–772 (1970).
14. E. CLEMENTI, H. KISTENMACHER, AND H. POPKIE, *J. Chem. Phys.* **58,** 2460–2466 (1973).
15. L. T. REDMON, G. D. PURVIS, AND R. J. BARTLETT, *J. Chem. Phys.* **72,** 986–991 (1980).
16. Z. K. ISMAIL, R. H. HANGE, AND J. L. MARGRAVE, *J. Chem. Phys.* **57,** 5137–5142 (1972).
17. M. J. WINTER AND W. J. JONES, *J. Chem. Soc. Faraday Trans. II* **78,** 585–594 (1982) and references therein.
18. P. K. PEARSON, H. F. SCHAEFER III, AND U. WAHLGREN, *J. Chem. Phys.* **62,** 350–354 (1982).
19. R. J. LE ROY AND J. VAN KRANENDONK, *J. Chem. Phys.* **61,** 4750–4769 (1974).
20. R. J. LE ROY AND J. S. CARLEY, *Adv. Chem. Phys.* **42,** 353–420 (1980).
21. J. TENNYSON AND A. VAN DER AVOIRD, *J. Chem. Phys.* **77,** 5664–5681 (1982).
22. S. CARTER AND N. C. HANDY, *J. Mol. Spectrosc.* **95,** 9–19 (1982).
23. J. TENNYSON AND B. T. SUTCLIFFE, *J. Chem. Phys.*, in press.
24. G. BROCKS, A. VAN DER AVOIRD, B. T. SUTCLIFFE, AND J. TENNYSON, *Mol. Phys.*, submitted.

25. A. R. EDMONDS, "Angular Momentum in Quantum Mechanics," 2nd ed., Princeton Univ. Press, Princeton, N. J., 1960.
26. A. M. ARTHURS AND A. DALGARNO, *Proc. R. Soc. London Ser. A* **256,** 540–551 (1960).
27. J. M. BROWN, J. T. HONGEN, K.-P. HUBER, J. W. C. JOLMS, I. KOPP, H. LEFREBVRE-BRION, A. J. MERER, D. A. RAMSAY, J. ROSTAS, AND R. N. ZARE, *J. Mol. Spectrosc.* **55,** 500–503 (1975).
28. S. L. HOLMGREN, M. WALDMAN, AND W. KLEMPERER, *J. Chem. Phys.* **69,** 1661–1669 (1978).
29. G. HERZBERG, "Molecular Spectra and Molecular Structure, Vol. 2: Infrared and Raman Spectra of Polyatomic Molecules," p. 132, 210, Van Nostrand, New York, 1945.
30. A. SCHIEDEKAMP, C. W. BOCK, AND P. GEORGE, *J. Mol. Struct.* **67,** 107–119 (1980).
31. K. YAMADA AND M. WINNEWISSER, *Z. Naturforsch.* **31a,** 139–144 (1976).
32. J. TENNYSON, *Chem. Phys. Lett.* **86,** 181–184 (1982).
33. J. TENNYSON, *Comput. Phys. Commun.*, in press.
34. G. BROCKS, J. TENNYSON, AND A. VAN DER AVOIRD, in preparation.
35. J. VAN VAALS, W. L. MEERTS, AND A. DYMANUS, to be published.